metals

MDPI

Article

Martensitic Transformation and Plastic Deformation of TiCuNiZr-Based Bulk Metallic Glass Composites

Honggang Sun [1], Kaikai Song [1,*], Xiaoliang Han [1,*], Hui Xing [2], Xuelian Li [1], Shenghai Wang [1], Jeong Tae Kim [3], Niraj Chawake [3], Tapabrata Maity [4], Li Wang [1] and Jürgen Eckert [3,4]

1 School of Mechanical, Electrical & Information Engineering, Shandong University, Weihai 264209, China; sunhg@sdu.edu.cn (H.S.); hunterlxl@163.com (X.L.); shenghaiw@163.com (S.W.); wanglihxf@sdu.edu.cn (L.W.)

2 Department of Physics, School of Science, Northwestern Polytechnical University, Xi'an 710072, China; huixing@nwpu.edu.cn

3 Erich Schmid Institute of Materials Science, Austrian Academy of Sciences, A-8700 Leoben, Austria; jeongtae.kim@oeaw.ac.at (J.T.K.); niraj.chawake@oeaw.ac.at (N.C.); juergen.eckert@unileoben.ac.at (J.E.)

4 Department Materials Physics, Montanuniversität Leoben, A-8700 Leoben, Austria; tapabrata.maity@unileoben.ac.at

* Correspondence: songkaikai8297@gmail.com (K.S.); hanxiaoliang92@163.com (X.H.); Tel.: +86-631-5688-338 (K.S.)

Received: 7 February 2018; Accepted: 16 March 2018; Published: 20 March 2018

Abstract: In this study, the microstructural evolution and mechanical properties of TiCuNiZr-based bulk metallic glass (BMGs) composites were systematically investigated in order to optimize both the strength and the ductility of BMGs. By tailoring the glass-forming compositions, TiCuNiZr-based BMG composites with different volume fractions of B2 (Ti,Zr)(Cu,Ni) crystals precipitating in the glassy matrix exhibit not only macroscopic ductility but also high strength as well as work-hardening, which is due to the formation of multiple shear bands and martensitic transformation during deformation. Optimized mechanical properties can be achieved when the crystalline volume fraction is at least higher than 44 vol. %, which is attributed to the sizeable difference between Young's moduli of the B2 (Ti,Zr)(Cu,Ni) crystals and the glassy matrix, and the precipitation of Ti_2Cu intermetallic compounds at the B2 crystal boundaries. Our study provides a complementary understanding of how to tailor mechanical properties of TiCu-based BMG composites.

Keywords: bulk metallic glasses; composites; martensitic transformation; shear bands; composites; mechanical properties

1. Introduction

As a prominent class of metallic materials, bulk metallic glasses (BMGs) have attracted significant attention due to their advantageous mechanical properties, including high strength, high hardness, and excellent wear resistance [1–5]. However, highly localized shear bands tend to be activated in the glassy matrix during deformation, leading to strain softening and the catastrophic failure of BMGs [1–5]. In an attempt to circumvent these drawbacks, BMG composites have been explored by introducing crystalline second phases into the glassy matrix [6,7]. Previous studies have focused on the development of ex-situ fabricated BMG composites, but subsequently in-situ developed BMG composites were found to be a more effective way to enhance the mechanical properties of BMGs [6–12], especially when ductile crystals precipitate in the glassy matrix. Up until now, a variety of alloy systems have been developed and a remarkable tensile ductility has been achieved for Ti-based and Zr-based BMG composites with the formation of dendrites in the glassy matrix by introducing Be as a micro-alloying element and adjusting the fabrication process [6,13–19]. However, these BMG

composites usually suffer from strong strain softening due to the lack of pronounced work-hardening during deformation. Even though the effect of strain softening can be reduced to some extent by tailoring the glass-forming compositions and microstructures, the typically weak work-hardening of ductile dendrites during deformation still cannot provide sufficient work-hardening [6,13–19].

Based on the concept of transformation-induced plasticity (TRIP), CuZr-based BMG composites were developed by introducing the ductile, shape memory B2 CuZr phase into the glassy matrix [20–26]. Such BMG composites exhibit high strength and good plasticity together with obvious work-hardening under compressive and tensile loading conditions [20–26]. In order to promote the further development of such shape memory BMG composites, a lot of research has been devoted to applying this concept to other glass-forming compositions [27–32]. Among them, Ti-based alloy systems are good candidates because of their low density, superior glass-forming ability (GFA), good corrosion resistance, and relatively high Young's modulus [33–35]. So far, TiCu-based BMG composites have been explored by introducing the B2 austenite phase into the glassy matrix, which indeed show high strength and good ductility as well as work-hardening [27–29,36,37]. Kim et al. found that a gradual, martensitic transformation occurs within bimodal-sized B2 crystals, inducing branching and the multiplication of shear bands in the glassy matrix during deformation [27–29,36–38]. However, in order to better understand the formation and deformation of TiCu-based BMG composites, more studies are necessary to understand the reason for the absence of tensile ductility. Furthermore, the effect of crystalline volume fractions on the mechanical properties of TiCu-based BMG composites should also be investigated. In the present work, the microstructures and mechanical properties of TiCuNiZr-based BMG composites with Hf, Si, and/or Sn micro-alloying additions are investigated and their corresponding deformation mechanism is analyzed.

2. Materials and Methods

$Ti_{45.5}Cu_{37.5}Ni_{7.5}Zr_{2.5}Hf_3Si_1Sn_3$ (T1), $Ti_{46.5}Cu_{37.5}Ni_{7.5}Zr_{2.5}Si_1Sn_5$ (T2), $Ti_{43.5}Cu_{37.5}Ni_{7.5}Zr_{2.5}Hf_3Si_1Sn_5$ (T3), $Ti_{42.5}Cu_{37.5}Ni_{7.5}Zr_{2.5}Hf_5Sn_5$ (T4), and $Ti_{41.5}Cu_{37.5}Ni_{9.5}Zr_{2.5}Hf_3Si_1Sn_5$ (T5) master alloys were fabricated by arc-melting appropriate amounts of the constituting elements (>99.9% purity) under a Ti-gettered argon atmosphere, respectively. The master alloys were remelted at least four times before suction casting in order to guarantee chemical homogeneity. From these master alloys the melt-spun ribbons were prepared by single-roller melt-spinning, using a custom-made melt spinner at a wheel rotating speed of 31.4 m/s. In addition, rods with a diameter of 2 mm were prepared by rapid solidification, using a custom-made suction-casting device under an argon atmosphere. Thermal analysis on the ribbons and rods was executed by differential scanning calorimetry (DSC, Perkin Elmer 8500, PerkinElmer Inc., Waltham, MA, USA) at heating and cooling rates of 20 K/min. Both the distributions and morphologies of the crystals in the glassy matrix were investigated using an optical microscope (OM, Zeiss Axiophot, Carl Zeiss (Shanghai) Co., Ltd., Shanghai, China). A phase analysis of the ribbons and rods was carried out by X-ray diffraction (XRD, Rigaku D/max-rB, Rigaku Corporation, Tokyo, Japan) in reflection geometry, a scanning electron microscopy (SEM, Gemini 1530, Carl Zeiss (Shanghai) Co., Ltd., Shanghai, China) combined with an energy dispersive X-ray spectroscopy (EDX), and a transmission electron microscopy (TEM, JEOL-2100, JEOL Ltd., Tokyo, Japan). The samples for the TEM measurements were prepared by a focused ion beam system (FIB, HELIOS NanoLab 600i, FEI Company, Hillsboro, OR, USA) set-up in a SEM. Room-temperature compression tests were performed on specimens with a height-to-diameter ratio of about 2:1 using an electronic universal testing machine (CMT 5305, MTS Systems (China) Co., Ltd., Shenzhen, China) at an initial strain rate of 2.5×10^{-4} s^{-1}. The compression tests were repeated at least three times to assure the reproducibility of the data. The surface and fracture morphologies of the samples after deformation were investigated by SEM. Moreover, a nanoindentation (Anton Paar CSM-NHT^2, Anton Paar GmbH, Graz, Austria) device was adopted to obtain the elastic properties of the B2 crystals and the glassy matrix. The maximum applied force was 50 mN while the loading rate was 100 mN/min. The holding

time at the maximum applied force was 10 s. Furthermore, the T1 rods were annealed at 1073 K for 12 h and then quenched into water in order to obtain fully crystalline B2 samples.

3. Results and Discussion

3.1. Phase Formation and Microstructural Features of Melt-Spun Ribbons and As-Cast Rods

As shown in Figure 1a, the XRD patterns of the melt-spun T1, T2, T3, and T4 ribbons with a thickness of about 40 ± 10 μm display broad diffraction maxima, representing a typical amorphous feature. When the cooling rate decreases by increasing the sample dimension to a 2 mm diameter, some B2 TiCu crystals precipitate in the glassy matrix (Figure 1b). The XRD patterns suggest that there is less of an amorphous phase in the T1 and T2 specimens than in the T3 and T4 specimens. In order to confirm the volume fraction of the amorphous phase, DSC measurements were conducted on the melt-spun ribbons and the as-cast samples, respectively (Figure 1c,d). As shown in Figure 1c, the melt-spun ribbons exhibit two or three crystallization events following the glass transition. The corresponding glass transition temperature (T_g), as well as the onset temperature and the first peak temperature of crystallization (i.e., T_x and T_{p1}) for the present ribbons and rods were measured and are listed in Table 1. The T_g values are higher than 685 K, the values of T_x are higher than 740 K, and the values of T_{rg} (=$T_x - T_g$) are larger than 50 K, implying a relatively high thermal stability of the present metallic glasses [39]. In agreement with the XRD patterns of the as-cast rods, the crystallization enthalpies of the T1 and T2 specimens during heating are smaller than those of the T3 and T4 specimens, while the glass transition events of the T1 and T2 rods become indistinct due to a pronounced partial crystallization (Figure 1d). Based on the ratio of the crystallization enthalpies of the as-cast rods and the fully amorphous ribbons, the crystalline volume fraction (f_{c1}) can be approximately determined to be 83.7 ± 5.8 vol. %, 86.9 ± 6.1 vol. %, 44.0 ± 7.9 vol. %, and 38.5 ± 8.6 vol. % for the as-cast T1, T2, T3, and T4 rods, respectively. Hence, compared with the T1 and T2 rods, the T3 and T4 rods obviously possess relatively larger volume fractions of the amorphous phase (Table 1).

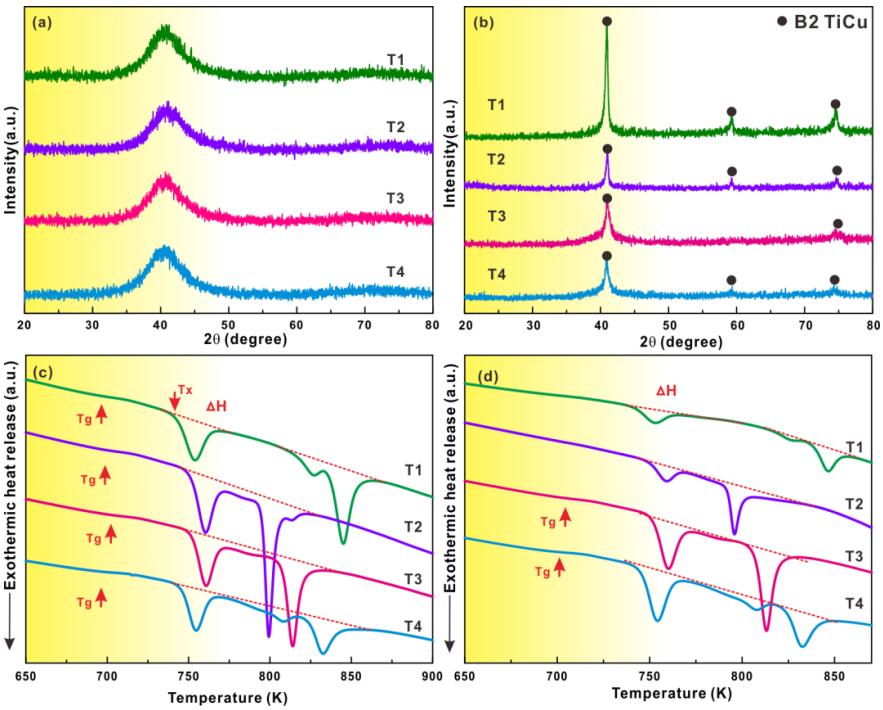

Figure 1. X-ray diffraction (XRD) patterns of the melt-spun T1, T2, T3, and T4 (**a**) ribbons and (**b**) rods with a diameter of 2 mm; differential scanning calorimetry (DSC) curves of the melt-spun T1, T2, T3, and T4 (**c**) ribbons and (**d**) rods.

Table 1. Values of T_g, T_x, and ΔT_{rg} for the melt-spun ribbons (recorded at 20 K/min heating rate) and the corresponding volume fractions of crystals f_{c1} and f_{c2} of the as-cast rods as determined from DSC measurements and optical microscopy, respectively.

Composition	T_g (K)	T_x (K)	ΔT_{rg} (K)	f_{c1} (vol. %)	f_{c2} (vol. %)
T1	689 ± 3	743 ± 1	54 ± 4	83.7 ± 5.8	85.5 ± 5.5
T2	693 ± 3	751 ± 1	58 ± 4	86.9 ± 6.1	70.0 ± 5.5
T3	692 ± 3	752 ± 1	60 ± 4	44.0 ± 7.9	37.7 ± 5.5
T4	687 ± 3	746 ± 1	59 ± 4	38.5 ± 8.6	37.4 ± 5.5

In order to further confirm the crystalline volume fraction and to illustrate both the distribution and morphology of the B2 crystals in the glassy matrix, OM and SEM measurements were performed on the rods (Figures 2 and 3), respectively. Based on the areas of the crystals in the glassy matrix, the crystalline volume fraction (f_{c2} in Table 1) showed a similar tendency as the f_{c1} values determined from calorimetry but exhibited small differences, which were most likely due to the slightly different cooling rates from the top to the bottom of the copper mold-cast rods [40,41]. As shown in Figure 2, the quasi-spherical crystals percolated with each other and only some crystals were isolated. It has been demonstrated that the percolation threshold in Cu-Zr-Al BMG composites lies between 30 and 50 vol. %, while for Zr-based BMG composites the threshold value is around 35 vol. % [42,43]. In our case, the critical f_c for the microstructural transition in the TiCu-based BMG composites is of the same order. As is well-known, it becomes easier for the amorphous phase to form at the surface of rods than in its center due to the gradual decrease of the cooling rate from the surface to the center [40,41]. Hence, when the applied cooling rate is a little lower than the critical cooling rate for full glass formation, crystals preferentially precipitate in the center of the sample while the amorphous phase (Figure 2) appears mostly at the surface of rods. Meanwhile, heterogeneous nucleation during solidification occurs at preferential sites, i.e., impurities from mold walls or at already solidified particles [44]. Consequently, some crystals also can precipitate on the mold surfaces due to the lower free energy barrier for nucleation even though the applied cooling rate is high enough to form fully amorphous samples. Consistent with previous results [28,36,38,42], some fine and isolated B2 crystalline particles were found in the glassy matrix beside the formation of a great amount of large, percolated crystals (Figure 2). Such bimodal length-scale crystalline particles should have a beneficial influence on the mechanical properties [28,36]. By magnifying the crystalline regions (Figure 3), a few precipitated intermetallic compounds were also detected around the B2 crystal boundaries (see the arrow). The EDX results show that some Zr, Ni, and other elements were dissolved in the B2 TiCu crystals, whose average chemical composition was roughly determined to be $Ti_{47.7}Cu_{36.4}Ni_{8.5}Zr_{1.6}Hf_{2.3}$ $Si_{0.9}Sn_{2.6}$ for the T1 specimen, as an example. Zhang et al. and Gargarella et al. reported that these precipitates are cubic B2 (Ti,Zr)(Cu,Ni) crystals [29,45].

In an attempt to confirm the existence of B2 and other unknown intermetallic phases in the glassy matrix, TEM measurements were performed on the as-cast T1 sample. As shown in Figure 4a, two kinds of different microstructural regions are observed. In region 1 (Figure 4b), some fine white intermetallic compounds (particles B) appear at the interface between particles A, which agrees well with SEM measurements. Based on the corresponding selected area electron diffraction (SAED) patterns (Figure 4c), the particles A are identified to be CsCl-type B2 crystals along the zone axis $[11\bar{1}]$. The particles B can be indexed as tetragonal Ti_2Cu (Figure 4d). In fact, different intermetallic compounds were also found in TiCu-based BMG composites, which strongly depend on the actual glass-forming compositions [27–29,36–38,46–49]. Zhang et al. and Chen et al. found that minor Sn addition can inhibit the precipitation of Ti_2Cu crystals, while some Cu_2ZrTi and Zr_5Sn_3 crystals also form with the addition of more Sn [46,47]. Gargarella et al. also reported Cu_2ZrTi intermetallic compounds together with a small amount of Ti_5Si_3 crystals [48], while the island-like Ti_2Cu intermetallic compounds precipitated within β-Ti dendrites [49]. Therefore, the thermal stability of intermetallic compounds can be effectively changed by tailoring the glass-forming compositions

and introducing different micro-alloying elements, leading to their precipitation in the glassy matrix. Furthermore, as shown in Figure 4e, some nano-scale twins were found in region 2. The corresponding SAED pattern (Figure 4f) further confirms the existence of twins (see the arrows), which can be identified as B19′ martensitic crystals by considering previous observations [27–29,36,37]. Figure 4g displays the distribution of the nano-scale twins, whose sizes are approximately between 20 and 80 nm. In general, the formation of martensite in the as-cast samples is expected to be induced by the internal stresses from quenching [50].

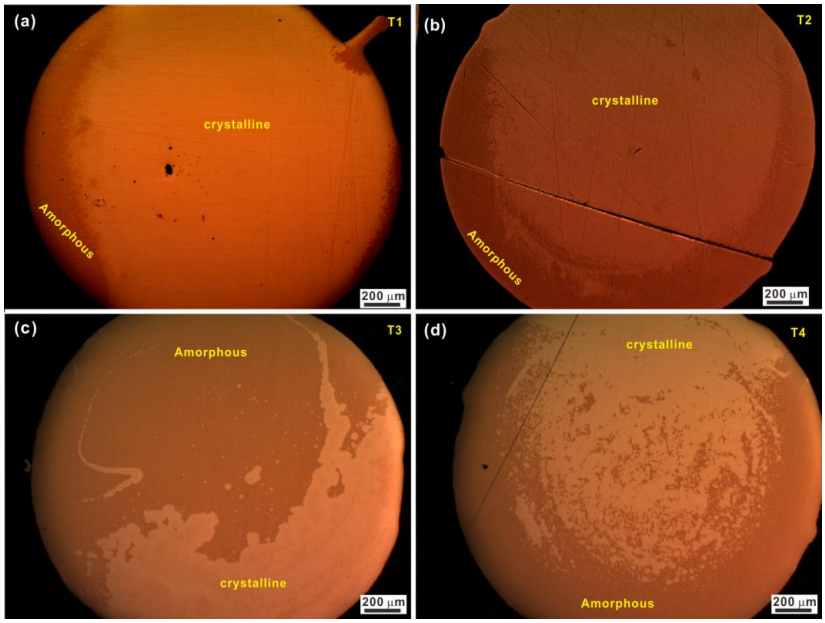

Figure 2. Optical microscope (OM) images of the as-cast (**a**) T1, (**b**) T2, (**c**) T3, and (**d**) T4 rods with a diameter of 2 mm.

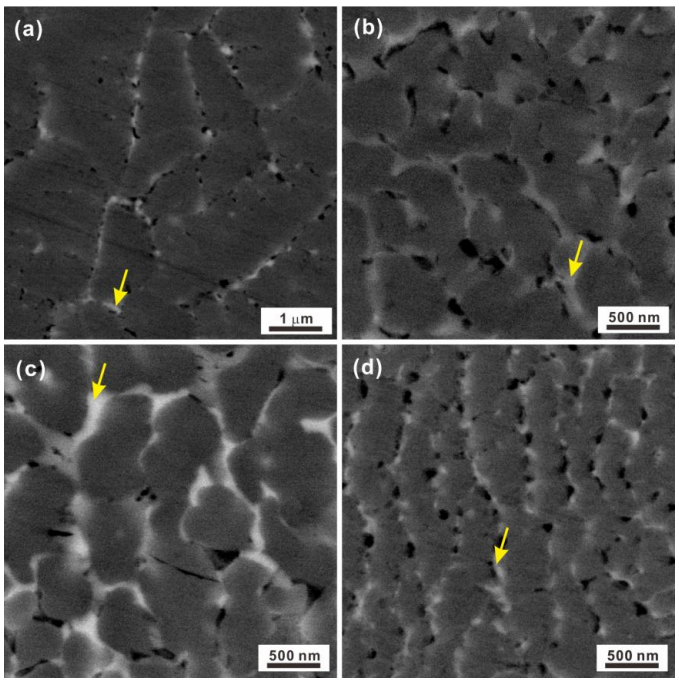

Figure 3. Backscattered scanning electron microscopy (SEM) images of crystals in the glassy matrix of the (**a**) T1, (**b**) T2, (**c**) T3, and (**d**) T4 rods.

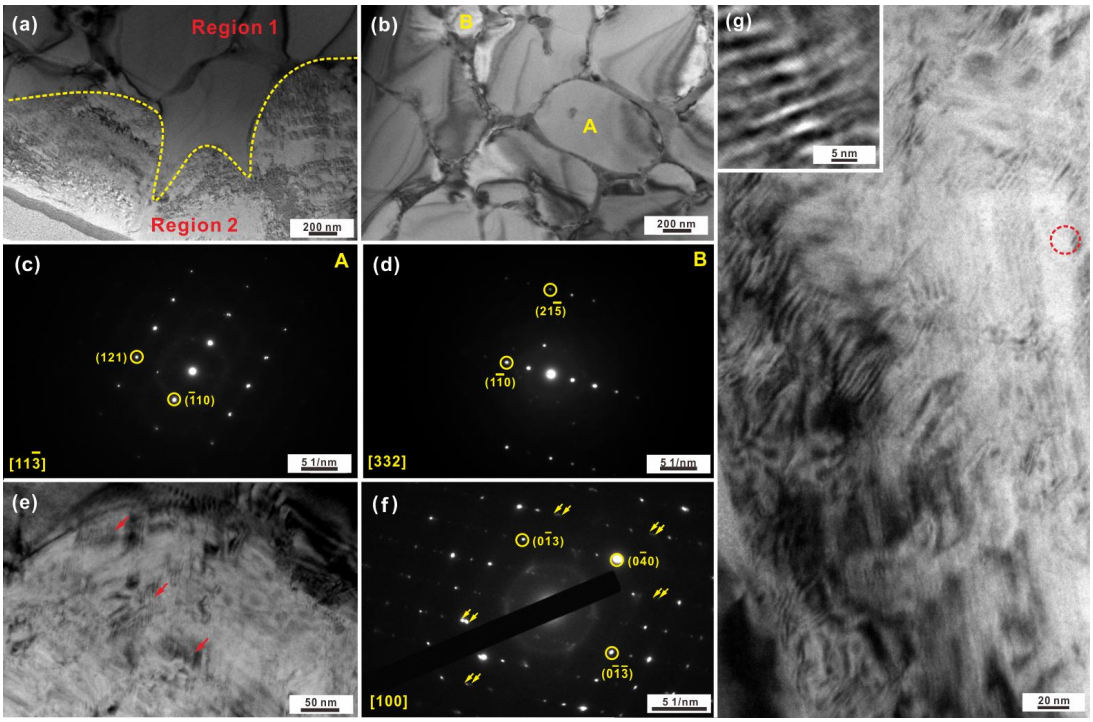

Figure 4. (**a**) Transmission electron microscopy (TEM) image of the T1 sample; (**b**) local enlarged image of region 1, selected area electron diffraction (SAED) patterns of particles; (**c**) particles A and (**d**) particles B; (**e**,**g**) local enlarged images of region 2 and the corresponding (**f**) SAED pattern.

3.2. Mechanical Properties of the As-Cast Rods

Figure 5a displays the engineering stress-strain curves of the as-cast T1, T2, T3, and T4 rods under compression. The values of the yield strength, the fracture strength, and the plastic strain of the investigated samples are listed in Table 2. With increasing crystalline volume fraction, both the plastic strain and the fracture strength gradually increase while the yield strength roughly decreases. When the f_c drops below 50 vol. %, the samples become brittle and only less than 3% plastic strain can be achieved for the T3 and T4 samples. The fracture angle deviates significantly from 45° and is closer to 90°. Even though a few multiple shear bands were still observed (Figure 5b), the number of shear bands is far less than the specimens with a f_c above 50 vol. % while some obvious cracks can be observed (see the dotted arrow). Meanwhile, many river-like patterns but only a few vein-like patterns were observed on their facture surfaces (Figure 5c). In fact, by further optimizing the glass-forming compositions, the GFA of TiCu-based BMG composites can be further enhanced in the $Ti_{41.5}Cu_{37.5}Ni_{9.5}Zr_{2.5}Hf_3Si_1Sn_5$ (T5) sample, whose structural features and deformation behaviors are displayed in the Supplementary materials (Figures S1 and S2). Only about 2 vol. % crystals uniformly distribute in the glassy matrix, which is identified as the B2 TiCu phase (Figure S1a,b). However, the compressive plastic strain is 0.7 ± 0.3%, together with a relatively high yield and fracture strength (Figure S1c). Furthermore, the fracture angle of the T5 samples also deviates significantly from 45° and is closer to 69°, while its corresponding fracture surface consists of smooth and vein pattern regions (Figure S2). Within the smooth regions, nanometer-scale "dimple" structures, which are the typical fracture features of some brittle Mg- and Fe-based BMGs, can be observed [51]. These brittle BMGs tend to fail in pieces or split and sometimes the facture angles are gradually closer to 90° for some samples, whose deformation is mainly governed by the crack-propagation. In our case, when the very limited f_c of ductile B2 crystals cannot effectively inhibit the rapid propagation of cracks, this results in the limited ductility of TiCu-based BMG composites.

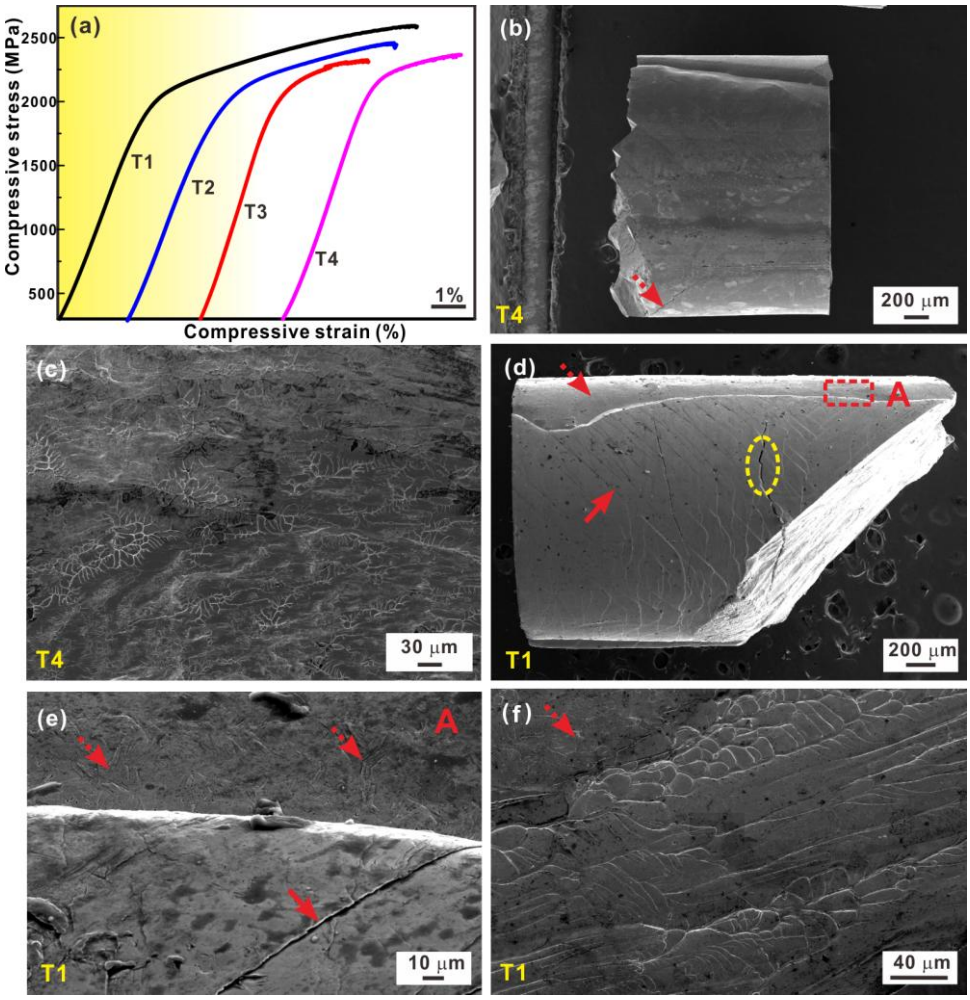

Figure 5. (**a**) Room temperature engineering stress-strain curves of the as-cast samples under compression; (**b**,**c**) the surface morphology and (**d**) the fracture morphology of the T1 sample after fracture; (**e**) the surface morphology and (**f**) the fracture morphology of the T4 sample.

Table 2. The values of the yield strength, the fracture strength, and the plastic strain of the investigated samples.

Composition	Yield Strength (MPa)	Fracture Strength (MPa)	Plastic Strain (%)
T1	1915 ± 45	2590 ± 45	7.7 ± 1.0
T2	1890 ± 35	2456 ± 35	5.3 ± 0.9
T3	1974 ± 15	2311 ± 15	2.6 ± 0.5
T4	2127 ± 15	2364 ± 15	2.4 ± 0.5

Additionally, the samples with a high f_c exhibit plastic strains larger than 5.0%, and fail in a shear mode (T1 in Figure 5d). The fracture angles are smaller than the main shear angle of 45°, i.e., 41 ± 2°. Since the amorphous phase forms mostly at the surface, a large amount of multiple shear bands can be observed (solid arrows in Figure 5d) as well as some cracks (dotted circle). At the interface between the amorphous phase and the crystals (see region A in Figure 5d), some martensitic crystals appear within the B2 crystals (dotted arrows in Figure 5e), implying the occurrence of martensitic transformation during deformation. The fracture morphologies (Figure 5f) show a number of vein-like and river-like patterns while some fine river-like patterns appear at the interface between the amorphous phase and the crystals, implying that the "blocking effect" [52]

originating from the crystals has a large influence on the fracture mode. Generally speaking, by introducing ductile shape memory crystals into the glassy matrix, the ductility of BMG composites can be improved [20–26]. During the early stage of deformation, martensitic transformation occurs within B2 crystals in CuZr-based BMG composites [20–26]. With increasingly applied stress, martensitic transformation becomes more prominent while a large amount of twins form easily within B2 crystals with a relatively lower stacking fault energy [53]. Meanwhile, the shear bands can dissolve precipitates, wrap around crystalline obstacles, or be blocked depending on the size and density of the precipitates, leading to the multiplication of shear bands in the glassy matrix [54]. Recently, Hong et al. have also observed such a deformation behavior in TiCu-based BMG composites [36]. Even though TiCu-based BMG composites with a similar f_c exhibit relatively higher yield strength than CuZr-based BMG composites, their room-temperature ductility is not as good as expected. Until now, no tensile ductility of TiCu-based BMG composites with precipitation of B2 crystals had been achieved in contrast to Ti-based BMG composites with a precipitation of ductile α-Ti or β-Ti dendrites in the glassy matrix [15,16,30–32,55]. Based on previous results [15,16,30–32,55], the tensile ductility of BMG composites strongly depended on the crystalline volume fraction, size, and distribution of crystals as well as on suitable glass-forming ability (GFA) [6,13–26]. Until now, several approaches were proposed to describe transformation toughening in BMG composites [42,56,57], among which the yield strength and fracture strain can be successfully described by a strength model considering both percolation and an empirical, three-microstructural-element-body approach, respectively. Then the correlation between yield strength/fracture strain and the f_c, especially in CuZr-based BMG composites [42], can be easily illustrated. For TiCu-based glass-forming alloys, both GFA and the formation of B2 TiCu crystals can be effectively optimized by controlling their compositions and the casting process [20–26]. However, by collecting both the yield strength and the fracture stains of TiCu-based BMG composites as well as the fully crystalline samples (Figure 6a), the strength model cannot well describe the f_c dependence of the yield strength and the fracture stain. Therefore, other factors except the volume fraction and distribution of B2 crystals should be considered for fabricating ductile TiCu-based BMG composites, namely, the precipitation of brittle intermetallic compounds and/or the thermal expansion misfit around the interfaces.

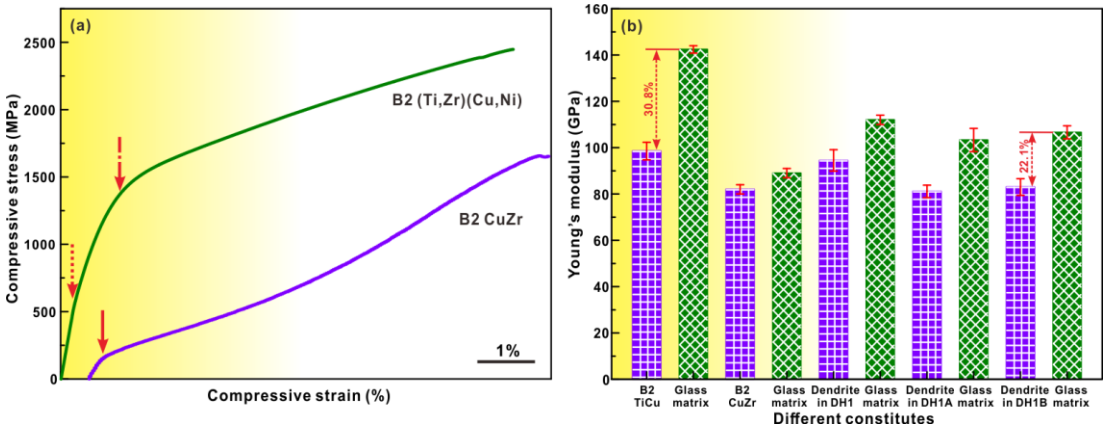

Figure 6. (**a**) The engineering stress-true strain curves under compression of shape memory B2 CuZr crystalline samples for $Cu_{47.5}Zr_{47.5}Al_5$ alloys and crystalline B2 (Ti,Zr)(Cu,Ni) specimens in the present work, and (**b**) Young's moduli of the dispersed particles and the matrix for TiCu-based, CuZr-based [42], and Zr-based BMG composites (i.e., DH1, DH1A, and DH1B) [55].

As shown in Figure 6a, the yield strength of B2 (Ti,Zr)(Cu,Ni) crystalline samples is far higher compared with B2 CuZr crystalline samples. During the elastic-plastic deformation stage, the martensitic transformation initiates at a stress of about 545 MPa (dotted arrow in Figure 6a) and further martensitic transformation occurs with increasing the applied stress to 1150 ± 20 MPa

(dash-dotted arrow in Figure 6a). The high yield strength of B2 (Ti,Zr)(Cu,Ni) crystals is linked to the precipitation of Ti_2Cu intermetallic compounds at the B2 crystal boundaries. For CuZr-based BMG composites, a few $Cu_{10}Zr_7$ and/or other intermetallic compounds also precipitate, which usually exist within B2 CuZr crystals but not at their interfaces [58]. The precipitation of fine intermetallic compounds around crystal boundaries can inhibit the rapid development of martensitic transformation to some degree [59,60]. Hence, in our case, the Ti_2Cu intermetallic compounds at the B2 crystal boundaries should play an important role on the mechanical properties. During deformation, less elastic energy of the TiCu-based BMG composites can be effectively released compared with CuZr-based BMG composites due to the inhibited martensitic transformation before the formation and propagation of shear bands in the glassy matrix.

On the other hand, the elastic mismatch between the dispersed particles and the matrix has a strong influence on the formation and propagation of shear bands and cracks [61]. Optimum toughness/ductility of the brittle composites can be achieved usually when the elastic rigidity moduli of the dispersed particles is equal to or less than that of the matrix and the interfacial bond strength is sufficient to allow a plastic deformation of the dispersed particles [61,62]. Murali et al. proposed that the normalized toughness of composites increases rapidly as the modulus mismatch decreases, approaching a maximum value as the modulus mismatch becomes close to zero [62]. Figure 6b displays Young's moduli of the dispersed particles and the matrix for TiCu-based, CuZr-based, and Zr-based BMG composites, respectively. It can be seen that the difference between B2 (Ti,Zr)(Cu,Ni) crystals and the glassy matrix is as large as approximately 30.8% while the difference of particles and matrix for other based BMG composites is between 7.8% and 22.1% [42,55]. Therefore, the modulus mismatch between B2 (Ti,Zr)(Cu,Ni) crystals and the glassy matrix in TiCu-based BMG composites is higher compared with other ductile BMG composites, which induces large residual stresses caused by thermal expansion misfit [63]. Therefore, even though the "blocking effect" originating from B2 crystals can induce the multiplication of shear bands at the interface between crystals and the glassy matrix, the subsequent shear banding instability may not be sufficiently decreased due to the large residual stresses at the interfaces, as a result micro-cracks easily appear. Meanwhile, the martensitic transformation cannot effectively continue to dissipate the elastic energy stored in the sample-machine systems during deformation. As a result, the mechanical properties of the present TiCu-based BMG composites are better than for TiCu-based BMGs but worse than for CuZr-based BMG composites when f_c is below 50 vol. %.

Therefore, in order to enhance the room-temperature ductility of TiCu-based BMG composites, a higher volume fraction of B2 crystals should be introduced into the glassy matrix compared with CuZr-based BMG composites. When the volume fraction of crystals in the glassy matrix is at least higher than 44 vol. %, relatively good ductility can be achieved while the yield strength maintains a higher value than 1800 MPa. In fact, when the crystalline volume fraction of CuZr-based and other ductile BMG composites is higher than 50 vol. %, their corresponding yield strength is reduced. In our case, the relatively high yield is due to the high yield strength of the B2 crystals and the precipitation of Ti_2Cu intermetallic compounds at the B2 crystal boundaries. During deformation, even though the Ti_2Cu intermetallic compounds restrain the development of martensitic transformation, a large amount of B2 crystals reduces this harmful effect to some content and the Ti_2Cu intermetallic compounds can also provide a precipitation strengthening effect on the mechanical properties of TiCu-based BMG composites, leading to relatively good mechanical properties.

4. Conclusions

In this work, TiCuNiZr-based BMG composites with micro-alloying elements and different crystalline volume fractions were fabricated by rapid solidification. The microstructure of the present composites is composed of B2 and glassy phases as well as a small amount of Ti_2Cu intermetallic compounds at the interface between B2 crystals and the glassy matrix. During deformation, martensitic transformation occurs within the B2 crystals and multiplication of the shear bands

can be induced, leading to not only macroscopic ductility but also high strength as well obvious work-hardening of the present BMG composites. In contrast to CuZr-based and other based ductile BMG composites, the difference between Young's moduli of B2 (Ti,Zr)(Cu,Ni) crystals and the glassy matrix is quite large, which induces a large elastic mismatch and increases the shear banding instability. Besides, some Ti_2Cu intermetallic compounds precipitating at the B2 crystal boundaries can inhibit martensitic transformation and then go against the elastic energy dissipation during deformation, which aggravates the shear banding instability. Hence, at least higher than 44 vol. % B2 crystals should be introduced into the glassy matrix in order to achieve optimized mechanical properties of TiCu-based BMG composites.

Supplementary Materials: The following are available online at http://www.mdpi.com/2075-4701/8/3/196/s1, Figure S1: (a) XRD pattern, (b) OM image, and (c) room temperature engineering stress-strain curves of the as-cast T5 samples under compression; Figure S2: (a) the surface morphology and (b–d) the fracture morphology of the as-cast T5 samples under compression.

Acknowledgments: The authors are grateful to K.L. Wang, J. Mi, Y.Q. Xin, S. Guo, and S.P. Hu for technical assistance and discussions. This work was supported by the National Natural Science Foundation of China (51761135125, 51501103 and 51501104), the German Science Foundation (DFG) under the Leibniz Program (EC 111/26-1), the European Research Council under the ERC Advanced Grant INTELHYB (ERC-2013-ADG-340025), and the Young Scholars Program of Shandong University at Weihai.

Author Contributions: K.S. and X.H. conceived and designed the experiments; H.S., X.H., and H.X. performed the experiments; K.S., H.S., L.W., J.T.K., N.C., T.M., and J.E. analyzed the data; X.L. and S.W. contributed analysis tools; K.S., H.S., and X.H. wrote the paper.

Conflicts of Interest: The authors declare no conflict of interest.

References

1. Schuh, C.A.; Hufnagel, T.C.; Ramamurty, U. Mechanical behavior of amorphous alloys. *Acta Mater.* **2007**, *55*, 4067–4109. [CrossRef]
2. Wang, W.H.; Dong, C.; Shek, C.H. Bulk metallic glasses. *Mater. Sci. Eng. R Rep.* **2004**, *44*, 45–89. [CrossRef]
3. Kim, D.H.; Kim, W.T.; Park, E.S.; Mattern, N.; Eckert, J. Phase separation in metallic glasses. *Prog. Mater. Sci.* **2013**, *58*, 1103–1172. [CrossRef]
4. Greer, A.L.; Cheng, Y.Q.; Ma, E. Shear bands in metallic glasses. *Mater. Sci. Eng. R Rep.* **2013**, *74*, 71–132. [CrossRef]
5. Egami, T.; Iwashita, T.; Dmowski, W. Mechanical properties of metallic glasses. *Metals* **2013**, *3*, 77–113. [CrossRef]
6. Qiao, J.W.; Jia, H.; Liaw, P.K. Metallic glass matrix composites. *Mater. Sci. Eng. R Rep.* **2016**, *100*, 1–69. [CrossRef]
7. Eckert, J.; Das, J.; Pauly, S.; Duhamel, C. Processing routes, microstructure and mechanical properties of metallic glasses and their composites. *Adv. Eng. Mater.* **2007**, *9*, 443–453. [CrossRef]
8. Choi-Yim, H.; Busch, R.; Köster, U.; Johnson, W.L. Synthesis and characterization of particulate reinforced $Zr_{57}Nb_5Al_{10}Cu_{15.4}Ni_{12.6}$ bulk metallic glass composites. *Acta Mater.* **1999**, *47*, 2455–2462. [CrossRef]
9. Choi-Yim, H.; Johnson, W.L. Bulk metallic glass matrix composites. *Appl. Phys. Lett.* **1997**, *71*, 3808–3810. [CrossRef]
10. Madge, V.S.; Louzguine-Luzgin, V.D.; Inoue, A.; Greer, L.A. Large compressive plasticity in a La-based glass-crystal composite. *Metals* **2013**, *3*, 41–48. [CrossRef]
11. Kim, J.Y.; Scudino, S.; Kühn, U.; Kim, B.S.; Lee, M.H.; Eckert, J. Production and characterization of brass-matrix composites reinforced with $Ni_{59}Zr_{20}Ti_{16}Si_2Sn_3$ glassy particles. *Metals* **2012**, *2*, 79–94. [CrossRef]
12. Bu, F.; Wang, J.; Li, L.; Kou, H.; Xue, X.; Li, J. The effect of thermal cycling treatments on the thermal stability and mechanical properties of a Ti-based bulk metallic glass composite. *Metals* **2016**, *6*, 274. [CrossRef]
13. Hofmann, D.C.; Suh, J.Y.; Wiest, A.; Lind, M.L.; Demetriou, M.D.; Johnson, W.L. Development of tough, low-density titanium-based bulk metallic glass matrix composites with tensile ductility. *Proc. Natl. Acad. Sci. USA* **2008**, *105*, 20136–20140. [CrossRef] [PubMed]

14. Hofmann, D.C.; Suh, J.Y.; Wiest, A.; Duan, G.; Lind, M.L.; Demetriou, M.D.; Johnson, W.L. Designing metallic glass matrix composites with high toughness and tensile ductility. *Nature* **2008**, *451*, 1085–1089. [CrossRef] [PubMed]
15. Qiao, J.W.; Sun, A.C.; Huang, E.W.; Zhang, Y.; Liaw, P.K.; Chuang, C.P. Tensile deformation micromechanisms for bulk metallic glass matrix composites: From work-hardening to softening. *Acta Mater.* **2011**, *59*, 4126–4137. [CrossRef]
16. Narayan, R.L.; Singh, P.S.; Hofmann, D.C.; Hutchinson, N.; Flores, K.M.; Ramamurty, U. On the microstructure-tensile property correlations in bulk metallic glass matrix composites with crystalline dendrites. *Acta Mater.* **2012**, *60*, 5089–5100. [CrossRef]
17. Hays, C.C.; Kim, C.P.; Johnson, W.L. Microstructure controlled shear band pattern formation and enhanced plasticity of bulk metallic glasses containing in situ formed ductile phase dendrite dispersions. *Phys. Rev. Lett.* **2000**, *84*, 2901–2904. [CrossRef] [PubMed]
18. Chen, G.; Cheng, J.L.; Liu, C.T. Large-sized Zr-based bulk-metallic-glass composite with enhanced tensile properties. *Intermetallics* **2012**, *28*, 25–33. [CrossRef]
19. Zhang, L.; Li, W.Q.; Zhu, Z.W.; Fu, H.M.; Li, H.; Li, Z.K.; Zhang, H.W.; Wang, A.M.; Zhang, H.F. Distribution of Be in a Ti-based bulk metallic glass composite containing β-Ti. *J. Mater. Sci. Technol.* **2017**, *33*, 708–711. [CrossRef]
20. Qin, Y.S.; Han, X.L.; Song, K.K.; Tian, Y.H.; Peng, C.X.; Wang, L.; Sun, B.A.; Wang, G.; Kaban, I.; Eckert, J. Local melting to design strong and plastically deformable bulk metallic glass composites. *Sci. Rep.* **2017**, *7*, 42518. [CrossRef] [PubMed]
21. Song, K.K.; Han, X.L.; Pauly, S.; Qin, Y.S.; Kosiba, K.; Peng, C.X.; Gong, J.H.; Chen, P.X.; Wang, L.; Sarac, B.; et al. Rapid and partial crystallization to design ductile CuZr-based bulk metallic glass composites. *Mater. Des.* **2018**, *139*, 132–140. [CrossRef]
22. Wu, F.F.; Chan, K.C.; Jiang, S.S.; Chen, S.H.; Wang, G. Bulk metallic glass composite with good tensile ductility, high strength and large elastic strain limit. *Sci. Rep.* **2014**, *4*, 5302. [CrossRef] [PubMed]
23. Wu, D.; Song, K.K.; Cao, C.D.; Li, R.; Wang, G.; Wu, Y.; Wan, F.; Ding, F.L.; Shi, Y.; Bai, X.J.; et al. Deformation-induced martensitic transformation in Cu-Zr-Zn bulk metallic glass composites. *Metals* **2015**, *5*, 2134–2147. [CrossRef]
24. Wu, Y.; Xiao, Y.; Chen, G.; Liu, C.T.; Lu, Z. Bulk metallic glass composites with transformation-mediated work-hardening and ductility. *Adv. Mater.* **2010**, *22*, 2770–2773. [CrossRef] [PubMed]
25. Han, X.; Qin, Y.; Qin, K.; Li, X.; Wang, S.; Mi, J.; Song, K.; Wang, L. Glass-forming ability and early crystallization kinetics of novel Cu-Zr-Al-Co. bulk metallic glasses. *Metals* **2016**, *6*, 225. [CrossRef]
26. Wu, Y.; Ma, D.; Li, Q.K.; Stoica, A.D.; Song, W.L.; Wang, H.; Liu, X.J.; Stoica, G.M.; Wang, G.Y.; An, K.; et al. Transformation-induced plasticity in bulk metallic glass composites evidenced by in-situ neutron diffraction. *Acta Mater.* **2017**, *124*, 478–488. [CrossRef]
27. Gargarella, P.; Pauly, S.; Samadi Khoshkhoo, M.; Kühn, U.; Eckert, J. Phase formation and mechanical properties of Ti-Cu-Ni-Zr bulk metallic glass composites. *Acta Mater.* **2014**, *65*, 259–269. [CrossRef]
28. Hong, S.H.; Kim, J.T.; Mun, S.C.; Kim, Y.S.; Park, H.J.; Na, Y.S.; Lim, K.R.; Park, J.M.; Kim, K.B. Influence of spherical particles and interfacial stress distribution on viscous flow behavior of Ti-Cu-Ni-Zr-Sn bulk metallic glass composites. *Intermetallics* **2017**, *91*, 90–94. [CrossRef]
29. Zhang, Z.Y.; Wu, Y.; Zhou, J.; Wang, H.; Liu, X.J.; Lu, Z.P. Strong work-hardening behavior in a Ti-based bulk metallic glass composite. *Scr. Mater.* **2013**, *69*, 73–76. [CrossRef]
30. Liu, D.; Zhu, Z.; Li, Z.; Zhang, L.; Fu, H.; Wang, A.; Li, H.; Zhang, H.; Wang, Y.; Zhang, H. Modulating work-hardening behaviors and tensile plasticity of in-situ formed ductile dendrite Ti-based bulk metallic glass composites with tailored dendrite composition. *Scr. Mater.* **2018**, *146*, 22–26. [CrossRef]
31. Oh, Y.S.; Kim, C.P.; Lee, S.; Kim, N.J. Microstructure and tensile properties of high-strength high-ductility Ti-based amorphous matrix composites containing ductile dendrites. *Acta Mater.* **2011**, *59*, 7277–7286. [CrossRef]
32. Zhang, L.; Zhang, H.F.; Li, W.Q.; Gemming, T.; Wang, P.; Bönisch, M.; Şopu, D.; Eckert, J.; Pauly, S. β-type Ti-based bulk metallic glass composites with tailored structural metastability. *J. Alloys Compd.* **2017**, *708*, 972–981. [CrossRef]

33. Kim, K.B.; Zhang, X.F.; Yi, S.; Lee, M.H.; Das, J.; Eckert, J. Effect of local chemistry, structure and length scale of heterogeneities on the mechanical properties of a $Ti_{45}Cu_{40}Ni_{7.5}Zr_5Sn_{2.5}$ bulk metallic glass. *Philos. Mag. Lett.* **2008**, *88*, 75–81. [CrossRef]
34. Shen, J.; Huang, Y.; Sun, J. Plasticity of a TiCu-based bulk metallic glass: Effect of cooling rate. *J. Mater. Res.* **2007**, *22*, 3067–3074. [CrossRef]
35. Wang, G.; Liu, Y.H.; Yu, P.; Zhao, D.Q.; Pan, M.X.; Wang, W.H. Structural evolution in TiCu-based bulk metallic glass with large compressive plasticity. *Appl. Phys. Lett.* **2006**, *89*, 251909. [CrossRef]
36. Hong, S.H.; Kim, J.T.; Park, H.J.; Kim, Y.S.; Suh, J.Y.; Na, Y.S.; Lim, K.R.; Park, J.M.; Kim, K.B. Gradual martensitic transformation of B2 phase on TiCu-based bulk metallic glass composite during deformation. *Intermetallics* **2016**, *75*, 1–7. [CrossRef]
37. Hong, S.H.; Kim, J.T.; Park, H.J.; Suh, J.Y.; Lim, K.R.; Na, Y.S.; Park, J.M.; Kim, K.B. Work-hardening and plastic deformation behavior of Ti-based bulk metallic glass composites with bimodal sized B2 particles. *Intermetallics* **2015**, *62*, 36–42. [CrossRef]
38. Hong, S.H.; Kim, J.T.; Lee, M.W.; Park, J.M.; Lee, M.H.; Kim, B.S.; Park, J.Y.; Seo, Y.; Suh, J.Y.; Yu, P.; et al. Combinatorial influence of bimodal size of B2 TiCu compounds on plasticity of Ti-Cu-Ni-Zr-Sn-Si bulk metallic glass composites. *Metall. Mater. Trans. A* **2014**, *45*, 2376–2381. [CrossRef]
39. Inoue, A. Stabilization of metallic supercooled liquid and bulk amorphous alloys. *Acta Mater.* **2000**, *48*, 279–306. [CrossRef]
40. Song, K.K.; Pauly, S.; Zhang, Y.; Li, R.; Gorantla, S.; Narayanan, N.; Kühn, U.; Gemming, T.; Eckert, J. Triple yielding and deformation mechanisms in metastable $Cu_{47.5}Zr_{47.5}Al_5$ composites. *Acta Mater.* **2012**, *60*, 6000–6012. [CrossRef]
41. Hermann, H.; Kokotin, V.; Eckert, J. Locally fluctuating cooling rate as possible reason for non-crystalline plasticity in metallic glasses. *Europhys. Lett.* **2012**, *98*, 16003. [CrossRef]
42. Pauly, S.; Liu, G.; Wang, G.; Kühn, U.; Mattern, N.; Eckert, J. Microstructural heterogeneities governing the deformation of $Cu_{47.5}Zr_{47.5}Al_5$ bulk metallic glass composites. *Acta Mater.* **2009**, *57*, 5445–5453. [CrossRef]
43. Fu, X.L.; Li, Y.; Schuh, C.A. Mechanical properties of metallic glass matrix composites: Effects of reinforcement character and connectivity. *Scr. Mater.* **2007**, *56*, 617–620. [CrossRef]
44. Glicksman, M.E. *Principles of Solidification: An Introduction to Modern Casting and Crystal Growth Concepts*, 1st ed.; Springer: New York, NY, USA, 2011.
45. Gargarella, P.; Pauly, S.; Khoshkhoo, M.S.; Kiminami, C.S.; Kühn, U.; Eckert, J. Improving the glass-forming ability and plasticity of a TiCu-based bulk metallic glass composite by minor additions of Si. *J. Alloys Compd.* **2016**, *663*, 531–539. [CrossRef]
46. Zhang, Z.Y.; Wu, Y.; Zhou, J.; Song, W.L.; Cao, D.; Wang, H.; Liu, X.J.; Lu, Z.P. Effects of Sn addition on phase formation and mechanical properties of TiCu-based bulk metallic glass composites. *Intermetallics* **2013**, *42*, 68–76. [CrossRef]
47. Chen, T.H.; Hsu, Y.K. Mechanical properties and microstructural of biomedical Ti-based bulk metallic glass with Sn addition. *Comput. Mater. Sci.* **2016**, *117*, 584–589. [CrossRef]
48. Gargarella, P.; Pauly, S.; Song, K.K.; Hu, J.; Barekar, N.S.; Samadi Khoshkhoo, M.; Teresiak, A.; Wendrock, H.; Kühn, U.; Ruffing, C.; et al. Ti-Cu-Ni shape memory bulk metallic glass composites. *Acta Mater.* **2013**, *61*, 151–162. [CrossRef]
49. Yang, S.; Li, D.; Li, X.C.; Zhang, Z.Z.; Zhang, S.F.; He, L. Composition dependence of the microstructure and mechanical behavior of Ti-Zr-Cu-Pd-Sn-Nb bulk metallic glass composites. *Intermetallics* **2017**, *90*, 1–8. [CrossRef]
50. Schryvers, D.; Firstov, G.S.; Seo, J.W.; Van Humbeeck, J.; Koval, Y.N. Unit cell determination in CuZr martensite by electron microscopy and X-ray diffraction. *Scr. Mater.* **1997**, *36*, 1119–1125. [CrossRef]
51. Xi, X.K.; Zhao, D.Q.; Pan, M.X.; Wang, W.H.; Wu, Y.; Lewandowski, J.J. Fracture of brittle metallic glasses: Brittleness or plasticity. *Phys. Rev. Lett.* **2012**, *109*, 245506. [CrossRef] [PubMed]
52. Wu, Y.; Wang, H.; Wu, H.H.; Zhang, Z.Y.; Hui, X.D.; Chen, G.L.; Ma, D.; Wang, X.L.; Lu, Z.P. Formation of Cu-Zr-Al bulk metallic glass composites with improved tensile properties. *Acta Mater.* **2011**, *59*, 2928–2936. [CrossRef]
53. Wu, Y.; Zhou, D.Q.; Song, W.L.; Wang, H.; Zhang, Z.Y.; Ma, D.; Wang, X.L.; Lu, Z.P. Ductilizing bulk metallic glass composite by tailoring stacking fault energy. *Phys. Rev. Lett.* **2012**, *109*, 245506. [CrossRef] [PubMed]

54. Brink, T.; Peterlechner, M.; Rösner, H.; Albe, K.; Wilde, G. Influence of crystalline nanoprecipitates on shear-band propagation in Cu-Zr-based metallic glasses. *Phys. Rev. Appl.* **2016**, *5*, 054005. [CrossRef]
55. Narayan, R.; Boopathy, K.; Sen, I.; Hofmann, D.; Ramamurty, U. On the hardness and elastic modulus of bulk metallic glass matrix composites. *Scr. Mater.* **2010**, *63*, 768–771. [CrossRef]
56. Corteen, J.; Rainforth, M.; Todd, I. A mathematical approach to transformation toughening in bulk metallic glasses. *Scr. Mater.* **2011**, *65*, 524–527. [CrossRef]
57. Pauly, S.; Liu, G.; Gorantla, S.; Wang, G.; Kühn, U.; Kim, D.H.; Eckert, J. Criteria for tensile plasticity in Cu-Zr-Al bulk metallic glasses. *Acta Mater.* **2010**, *58*, 4883–4890. [CrossRef]
58. Okulov, I.V.; Soldatov, I.V.; Sarmanova, M.F.; Kaban, I.; Gemming, T.; Edstrøm, K.; Eckert, J. Flash joule heating for ductilization of metallic glasses. *Nat. Commun.* **2015**, *6*. [CrossRef] [PubMed]
59. Otsuka, K.; Ren, X. Physical metallurgy of Ti-Ni-based shape memory alloys. *Prog. Mater. Sci.* **2005**, *50*, 511–678. [CrossRef]
60. Zhao, Y.; Wang, J.; Zhou, S.; Wang, X. Effects of rare earth addition on microstructure and mechanical properties of a Fe-15Mn-1.5Al-0.6C TWIP steel. *Mater. Sci. Eng. A* **2014**, *608*, 106–113. [CrossRef]
61. Khaund, A.K.; Nicholson, P.S. Fracture of a brittle composite: Influence of elastic mismatch and interfacial bonding. *J. Mater. Sci.* **1980**, *15*, 177–187. [CrossRef]
62. Murali, P.; Bhandakkar, T.K.; Cheah, W.L.; Jhon, M.H.; Gao, H.; Ahluwalia, R. Role of modulus mismatch on crack propagation and toughness enhancement in bioinspired composites. *Phys. Rev. E* **2011**, *84*, 015102. [CrossRef] [PubMed]
63. He, M.Y.; Evans, A.G.; Hutchinson, J.W. Crack deflection at an interface between dissimilar elastic materials: Role of residual stresses. *Int. J. Solids Struct.* **1994**, *31*, 3443–3455. [CrossRef]